Letter

Electrical Detection of Antiferromagnetic Dynamics in Gd-Co Thin Films Using 154-GHz Gyrotron Irradiation

S. Funada,[1] Y. Ishikawa,[2] M. Kimata,[3] K. Hayashi,[2] T. Sano,[2] K. Sugi,[1] Y. Fujii,[2] S. Mitsudo,[2]
Y. Shiota,[1,4] T. Ono,[1,4] and T. Moriyama[1,4,5,*]

[1]*Institute for Chemical Research, Kyoto University, Uji, Kyoto 611-0011, Japan*

[2]*Research Center for Development of Far-Infrared Region, University of Fukui, Fukui, Fukui 910-8507, Japan*

[3]*Institute for Materials Research, Tohoku University, Sendai, Miyagi 980-8577, Japan*

[4]*Center for Spintronics Research Network, Kyoto University, Uji, Kyoto 611-0011, Japan*

[5]*PRESTO, Japan Science and Technology Agency, Kawaguchi, Saitama 322-0012, Japan*

Terahertz (THz) magnetization dynamics is a key property of antiferromagnets and ferrimagnets that could harness the THz forefront and spintronics. While most of the present THz measurement techniques are for bulk materials, the sensitivities of which rely on the volume of material, measurement techniques suitable for thin films are quite limited. In this study, we explore and demonstrate the electrical detection of the antiferromagnetic dynamics in ferrimagnetic Gd-Co thin films by using a 154-GHz gyrotron, which is a high-power electromagnetic wave source. Captured resonant modes allow us to characterize the peculiar magnetization dynamics of Gd-Co around the net angular momentum compensation. As the gyrotron frequency is scalable up to THz, our demonstration is a milestone toward THz measurements for antiferro- and ferrimagnetic thin films.

Antiferromagnets are one of the promising magnetic materials that can sustain and work at terahertz (THz) frequency [1]. Amid antiferromagnetic-ferrimagnetic spintronics [2–5], where antiferromagnets and ferrimagnets are used as active materials in spintronic devices, the THz magnetization dynamics of antiferromagnets and ferrimagnets is a key property that can harness the THz forefront and spintronics. Recent advances in THz measurement techniques have realized some key experiments on the antiferromagnetic dynamics and relevant phenomena, such as control of THz spin oscillation [6–8], the THz spin-pumping effect [9], and ultrafast spin switching [10,11].

However, the measurement principles used in those studies, such as the magneto-optical effect and resonant absorption, rely on the volume of the materials. Therefore, the same principle can hardly be applied for characterizing the dynamics of thin films, which is a central interest when considering any antiferro- and ferrimagnetic integration devices. Indeed, due to the measurement difficulty, the basic properties of magnetization dynamics in antiferromagnetic thin films, such as resonant frequency and magnetic damping constant, remain elusive while, it is not perhaps legitimate to assume that these properties are same as those in bulk materials. Therefore, the establishment of

a measurement technique for characterizing antiferromagnetic dynamics in thin films is a pressing issue for THz spintronics.

Electrical detection of the magnetic resonance is one of the routes to establishing such a measurement technique. For ferromagnetic thin films, there are wide varieties of electrical measurement techniques that capture the magnetization dynamics. For instance, the homodyne detection technique, taking advantage of the nonlinear coupling between a rf current and a magnetoresistance oscillation [12–14], is widely used to characterize the dynamics in ferromagnetic thin films. The resultant electrical signal can be expressed as $\mathbf{V} = (\Delta\rho/\mathbf{M}^2)(\mathbf{J} \cdot \mathbf{M})\mathbf{M} - R_H\mathbf{J} \times \mathbf{M}$, where $\Delta\rho$ is the resistance change due to magnetoresistance, $\mathbf{M}$ is the magnetization, $\mathbf{J}$ is the current induced by electromagnetic wave irradiation, and R_H is the anomalous Hall effect constant. The technique not only characterizes ferromagnetic films as thin as subnanometers [15], but can also characterize various interesting nonequilibrium phenomena, such as spin torque [16]. Another is the spin-to-charge conversion technique, which takes advantage of a combination of the spin-pumping effect and the inverse spin Hall effect in a bilayer composed of ferromagnet/spin Hall metal, where the spin Hall metal is Pt, Ta, etc. [17,18]. Persistent magnetization dynamics in the ferromagnetic layer creates and pumps a spin current into the spin Hall metal layer by the spin-pumping effect. The spin

*mtaka@scl.kyoto-u.ac.jp

current injected in the spin Hall metal layer is converted into a charge current by which electrical detection of the magnetization dynamics is realized. The principle of the latter technique was recently demonstrated in particular bulk-antiferromagnet/spin Hall metal interfaces [19,20], i.e., MnF_2/Pt and Cr_2O_3/Pt; this strongly suggests that the characterization of thin films is possible.

An electrical signal, or more precisely a dc voltage signal, emerging at the resonance for both techniques is, in principle, proportional to the power of the input electromagnetic wave. Considering the case for ferromagnets, a sizable input microwave power (>mW) is generally required to obtain a comfortably detectable voltage signal of the order of μV [14,18]. A concern when it comes to the THz frequency is that such high-power continuous-wave (cw) THz sources are quite limited. The gyrotron is one of the few cw THz sources that can produce a power of >mW [21]. It consists of a linear-beam vacuum tube, in which the electron beam undergoes cyclotron resonance in a strong magnetic field. The cyclotron motion of the electrons emits electromagnetic waves at the resonant frequency and its higher harmonics. It is lab-size equipment and more accessible than other technologies, such as the free-electron laser [22].

Here, we explore the electrical detection of antiferromagnetic resonant modes in Gd_xCo_{1-x}/Ta and Gd_xCo_{1-x}/Pt thin films by employing a gyrotron that can generate 154 GHz with a nominal power of 500 mW. We clearly detect the resonances as a voltage signal, through which the characteristic magnetization dynamics of the Gd-Co alloy and its temperature dependence are discussed.

Bilayers of $Gd_{0.17}Co_{0.83}$(20 nm)/Ta(3 nm) (sample A), $Gd_{0.16}Co_{0.84}$(20 nm)/Pt(3 nm) (sample B), and $Gd_{0.16}Co_{0.84}$(20 nm)/Ta(3 nm) (sample C) are deposited on thermally oxidized Si substrates by magnetron sputtering with a base pressure of 1.5×10^{-6} Pa. Gd_xCo_{1-x} layers are formed by cosputtering of Gd and Co, and the composition is controlled by the sputtering power for each element. The Ta and Pt capping layer is to protect the Gd-Co layer from oxidation and to utilize the inverse spin Hall effect. Gd-Co alloys are one of the typical rare-earth–transition-metal ferrimagnets that show both magnetization and angular momentum compensation temperatures due to the difference in the temperature dependences of the magnetic moment and the gyromagnetic ratio of Gd to Co. The Gd-Co alloys generally show two dynamic modes due to the antiferromagnetically coupled magnetic sublattices of Gd and Co [23,24]. Peculiar magnetization dynamics in the vicinity of these compensation temperatures are comprehended by nonzero angular momentum with zero magnetization and vice versa [25–28].

Figure 1(a) shows the schematic of the measurement setup with a gyrotron. The 154-GHz continuous electromagnetic wave with a nominal power of 500 mW is generated by a gyrotron and guided into a hollow waveguide sticking out of a cryostat with a superconducting magnet. The electromagnetic wave is linearly polarized by a wire grid placed in the pathway. The sample shaped as a 1.5×5 mm^2 rectangular piece is placed at the end of the waveguide such that the Poynting vector of the electromagnetic wave is parallel to both the sample surface and the sample's transverse direction. The linearly polarized rf h field is aligned perpendicular to the sample plane. Voltage is measured across the sample's longitudinal direction with a sweeping external magnetic field, H_{ext}, colinear to the Poynting vector. The field direction opposite to the Poynting vector is defined as the positive field, as shown in Fig. 1(a).

Figure 1(b) shows typical spectra for sample A, with the Ta capping layer, at room temperature with negative and positive magnetic fields. Clear dc voltage peaks are observed, and there are two resonant modes at around ± 2 and ± 4 T. The peaks at around ± 4 T (labeled as $\star$) are larger than those at around ± 2 T (labeled as $\triangle$), and the polarities of the peak voltages are opposite to each other. For both modes, the polarity of the peak voltage is reversed when the magnetic field is reversed, which suggests that the dc voltage is from the magnetic resonances of Gd-Co.

First, we discuss the origin of the dc voltage peak. As discussed above, there are two possible detection mechanisms in our measurement configuration, i.e., the homodyne mechanism and the spin-pumping mechanism, that create the dc voltage at the resonance. If the spin-pumping mechanism were dominant, sample B, with the Pt capping layer, and sample C, with the Ta capping layer, would show opposite voltage polarities at the resonance because the signs of the spin Hall angles for Pt and Ta are opposite to each other [29,30]. As shown in Fig. 1(c), the voltage polarity at the resonance is the same for both samples B and C, indicating that the dominant mechanism is not spin pumping but the homodyne caused by nonlinear coupling between the induction current and the magnetoresistance of the Gd-Co film. A slight difference in the line shape between samples could come from a misalignment of the rf h field with respect to the sample geometry, as the line shape is quite sensitive to the alignment with the homodyne mechanism [13,31].

Next, we discuss the temperature dependence of the resonant modes. Figure 2(a) shows the spectra for sample A at various temperatures. We observe a clear dc voltage peak shifting in the range between 4 and 2 T with decreasing temperature. Figure 2(b) summarizes the resonant field, $\mu_0 H_{res}$, and resonant linewidth, $\mu_0 \Delta H_{res}$, which are extracted by Lorentzian peak fitting, as a function of temperature. $\mu_0 H_{res}$ decreases with decreasing temperature, and $\mu_0 \Delta H_{res}$ varies with respect to temperature and has a maximum at around 100 K.

Associated with the temperature-dependent magnetization and the temperature-dependent angular momentum, Gd-Co alloys generally show a strong temperature
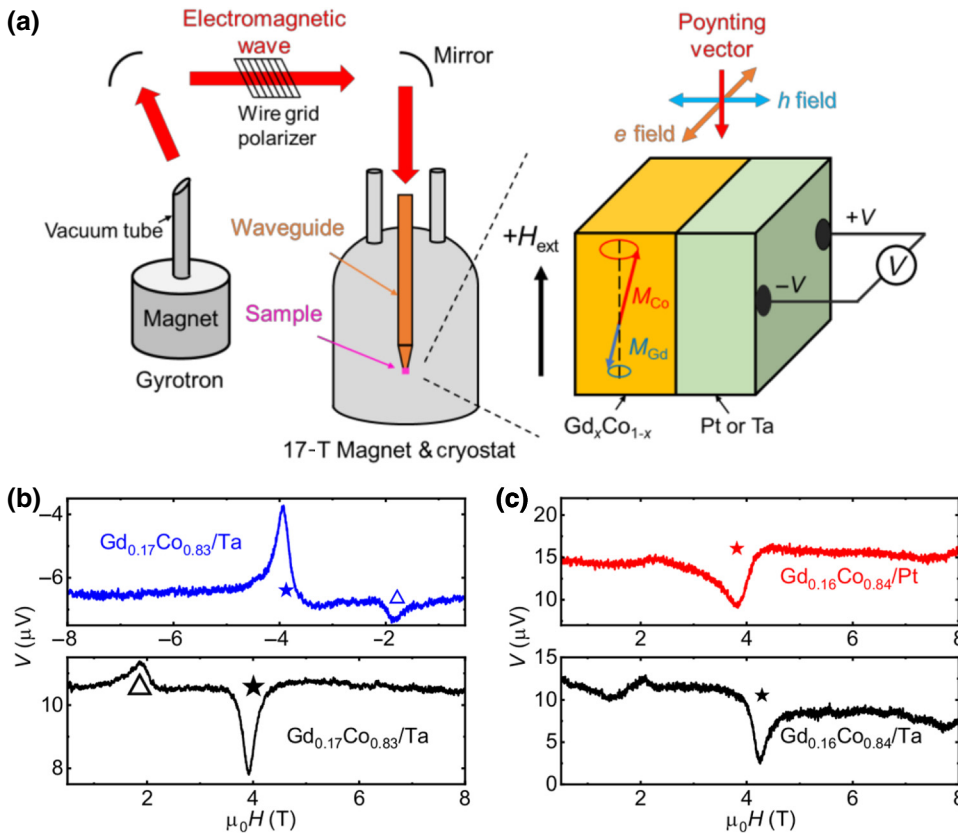
FIG. 1. (a) Schematic illustration of the measurement setup. 154-GHz electromagnetic wave is generated by the gyrotron and irradiated to the sample. Dc voltage across the sample is measured with sweeping external magnetic field. (b) Typical dc voltage spectra with negative and positive magnetic fields for sample A [$Gd_{0.17}Co_{0.83}$(20 nm)/Ta(3 nm)] at room temperature. (c) Dc voltage spectra for sample B [$Gd_{0.16}Co_{0.84}$ > (20 nm)/Pt(3 nm)] and sample C [$Gd_{0.16}Co_{0.84}$(20 nm)/Ta(3 nm)] at room temperature. ⋆ and △ label larger and smaller peaks, respectively.

dependence of the resonant frequency. Here, we define the temperature-dependent net magnetization, $M(T)$, and net angular momentum, $s_{net}(T)$, as [32]

$$M(T) = M'_{Co}(1 - T/T_c)^{\beta_{Co}} - M'_{Gd}(1 - T/T_c)^{\beta_{Gd}}, \quad (1)$$

$$s_{net}(T) = M'_{Co}/\gamma_{Co}(1 - T/T_c)^{\beta_{Co}} \\ - M'_{Gd}/\gamma_{Gd}(1 - T/T_c)^{\beta_{Gd}}, \quad (2)$$

where T_c is the critical temperature for the ferrimagnetic-paramagnetic transition, and $M'_{Gd,Co}$ and $\beta_{Gd,Co}$ are the magnetization at 0 K and the critical exponent, respectively, for each element. $\gamma_{Gd,Co} = g_{Gd,Co}\mu_B/\hbar$ is the gyromagnetic ratio, with the Bohr magneton, μ_B; reduced Planck's constant, $\hbar$; and g factor, $g_{Gd,Co}$, for each element. By obtaining $M'_{Gd,Co}$ and $\beta_{Gd,Co}$ from measured $M(T)$,

$s_{net}(T)$ can be estimated using the literature values of $g_{Gd} = 2.02$ and $g_{Co} = 2.11$ [33].

Figure 3 shows the measured $M(T)$ for sample A with a magnetization compensation temperature of $T_M \sim 40$ K. The obtained $s_{net}(T)$ is overlaid in Fig. 3. The angular momentum compensation temperature, T_A, is found to be 130 K. Resonant linewidths in Gd-Co are theoretically predicted to increase as the temperature approaches T_A. As we see in Fig. 2(b), $\mu_0\Delta H$ peaking at 100 K, roughly corresponding to the estimated T_A, is consistent with theory [34] and previous experimental observations [23,35].

Ferrimagnetic dynamics is essentially described by two sets of Landau-Lifshitz-Gilbert (LLG) equations for each magnetic sublattice of Gd and Co. When solving the simultaneous equation using the Neel vector basis, one obtains the eigenfrequencies [36,37]:
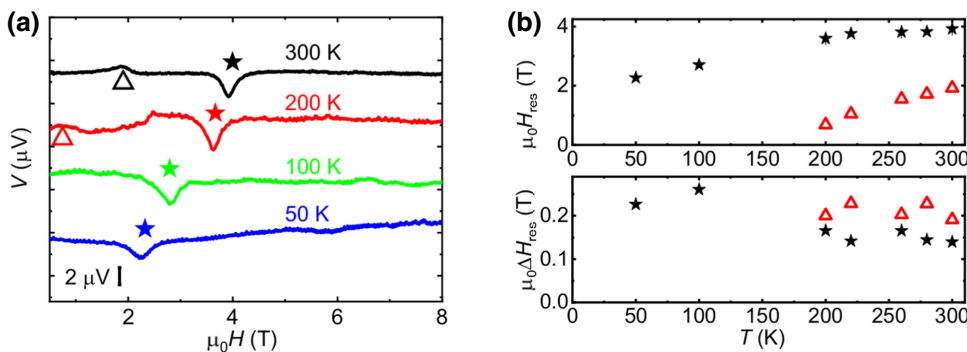

FIG. 2. (a) Dc voltage spectra at various temperatures for sample A. (b) Temperature dependence of the resonant field, $\mu_0 H_{res}$, and linewidth, $\mu_0\Delta H_{res}$, for the resonant peaks labeled as ⋆ and △. Data markers correspond to the labels of Fig. 1(b).

$$(f^{\pm})^2 = \frac{s_{\text{net}}^2 + \rho\mu_0 M(2H_{\text{ext}} + M) \pm \sqrt{s_{\text{net}}^4 + 2\rho s_{\text{net}}^2 \mu_0 M(2H_{\text{ext}} + M) + \rho^2(\mu_0 M)^2(M)^2}}{2(2\pi\rho)^2}, \qquad (3)$$

where f^- and f^+ indicate the low-frequency mode and high-frequency mode, respectively; and ρ is the momentum of inertia [38]. μ_0 is the vacuum permeability. With Eq. (3), $s_{\text{net}}(T)$ can also be obtained at each temperature by using the obtained H_{res}, $M(T)$, and $f^{\pm} = 154$ GHz with the literature value of $\rho = 2 \times 10^{-19}$ kg m^{-1} [37].

Figure 4 shows $s_{\text{net}}(T)$ estimated from Eq. (3) and that estimated from Eq. (2) with the measured $M(T)$ (taken from Fig. 2). Data points of blue and red squares are obtained for the larger resonant peaks (labeled as $\star$) by setting $f^- = 154$ GHz and $f^+ = 154$ GHz, respectively. There are no solutions of $s_{\text{net}}(T)$ for the smaller peaks (labeled as $\triangle$), indicating that these peaks may be associated with nonuniform magnetization modes or spin-wave modes. Values of $s_{\text{net}}(T)$ obtained in two different ways are roughly consistent with each other. In addition, this calculation identifies that observed resonant peaks are from the low-frequency mode above T_A and high-frequency mode below T_A.

These results invoke the immediate question why there is only one mode at given temperatures. To address this issue, we introduce the concept of handedness for magnetization dynamics. When solving the set of LLG equations using the elliptical basis of each sublattice magnetization, one then finds $f^- = f_R$ and $f^+ = f_L$ at $T > T_A$ and $f^- = f_L$ and $f^+ = f_R$ at $T_M < T < T_A$, in comparison with Eq. (3) [24], where f_R and f_L are, respectively, the resonant frequency for the right-handed and left-handed precession modes with respect to a principal axis parallel to the net magnetization. This analysis indeed reveals the resonant peaks we observe are always the right-handed modes throughout the temperature range. We therefore find that the left-handed modes are invisible in our experiment.
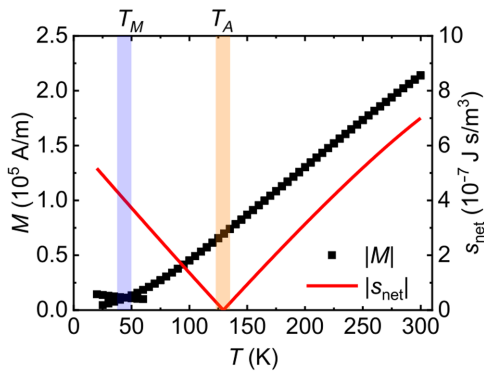
In most of the previous experimental studies on Gd-Co dynamics, contrary to our results, the two modes at a given temperature are clearly identified [23,24]. We suspect the reason why we do not see the left-handed modes might be rooted in how the dynamics is excited. Those previous studies used either the pump-probe technique or Brillouin light scattering (BLS). The pump-probe technique thermally excites the magnetization dynamics and BLS occurs through energy and momentum transfer from photons; neither excitation mechanism is directly relevant to the magnetic susceptibility. On the other hand, in the present measurement, the dynamics is purely driven by the rf h field. Therefore, magnetic susceptibility is an important factor in efficiently exciting the magnetization dynamics in the present study. Indeed, the magnetic susceptibility at f_L is found to be smaller than that at f_R, and they can differ by as much as a factor of 10 (see the Supplemental Material [39–45]), which could explain why the resonant peaks of the left-handed mode are too small to be seen in our experiment.

Finally, we would like to discuss the measurement configuration. Since the homodyne mechanism seems to be dominant in our measurement, it is possible to further enhance and maximize the dc voltage signal by looking into the correct geometry of the applied-field direction and the rf h-field directions with respect to the sample [14,31], which in the present study cannot be realized due to various geometrical limitations in the measurement setup but will be optimized in future work.
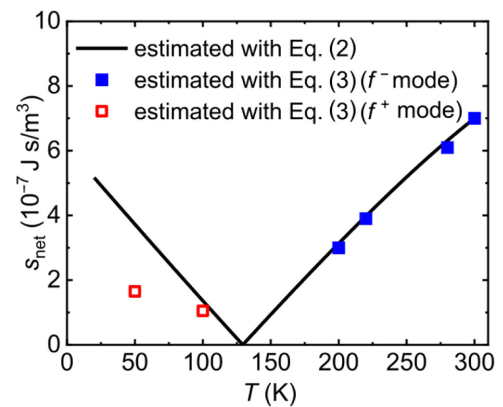

FIG. 4. Comparison of $s_{\text{net}}(T)$ estimated by Eqs. (2) and (3). Blue and red squares are obtained for the resonant peaks [labeled as $\star$ in Fig. 2(a)] by setting $f^- = 154$ GHz and $f^+ = 154$ GHz in Eq. (3), respectively. Black line shows $s_{\text{net}}(T)$ estimated by Eq. (2).

FIG. 3. Measured $M(T)$ for sample A under the in-plane magnetic field of 100 mT and $s_{\text{net}}(T)$ estimated by Eq. (2).

In summary, we demonstrate the electrical detection of magnetic resonance in Gd-Co ferrimagnetic thin films at 154 GHz by employing the gyrotron as a high-power electromagnetic wave source. It is found that the dc voltage peaks are predominantly from the homodyne mechanism. The temperature dependence of the resonant modes is well explained by the temperature dependence of the net angular momentum in Gd-Co. The lack of left-handed resonant modes in our observation could be related to the significant difference in the magnetic susceptibilities of the right- and left-handed modes. Since homodyne detection is a common effect in magnetic films with appreciable magnetoresistance, and the gyrotron frequency is scalable up to THz [21], our demonstration is a milestone toward THz measurements for antiferro- and ferrimagnetic thin films.

[1] D. M. Mittleman, Perspective: Terahertz science and technology, J. Appl. Phys. **122**, 230901 (2017).

[2] V. Baltz, A. Manchon, M. Tsoi, T. Moriyama, T. Ono, and Y. Tserkovnyak, Antiferromagnetic spintronics, Rev. Mod. Phys. **90**, 015005 (2018).

[3] T. Jungwirth, X. Marti, P. Wadley, and J. Wunderlich, Antiferromagnetic spintronics, Nat. Nanotechnol. **11**, 231 (2016).

[4] O. Gomonay, T. Jungwirth, and J. Sinova, Concepts of antiferromagnetic spintronics, Phys. Status Solidi RRL **11**, 1700022 (2017).

[5] S. K. Kim, G. S. D. Beach, K.-J. Lee, T. Ono, T. Rasing, and H. Yang, Ferrimagnetic spintronics, Nat. Mater. **21**, 24 (2022).

[6] T. Kampfrath, A. Sell, G. Klatt, A. Pashkin, S. Ma, T. Dekorsy, M. Wolf, M. Fiebig, A. Leitenstorfer, and R. Huber, Coherent terahertz control of antiferromagnetic spin waves, Nat. Photonics **5**, 31 (2011).

[7] T. Satoh, S. J. Cho, R. Iida, T. Shimura, K. Kuroda, H. Ueda, Y. Ueda, B. A. Ivanov, F. Nori, and M. Fiebig, Spin Oscillations in Antiferromagnetic NiO Triggered by Circularly Polarized Light, Phys. Rev. Lett. **105**, 077402 (2010).

[8] S. Baierl, M. Hohenleutner, T. Kampfrath, A. K. Zvezdin, A. v. Kimel, R. Huber, and R. v. Mikhaylovskiy, Nonlinear spin control by terahertz-driven anisotropy fields, Nat. Photonics **10**, 715 (2016).

[9] T. Moriyama, K. Hayashi, K. Yamada, M. Shima, Y. Ohya, Y. Tserkovnyak, and T. Ono, Enhanced antiferromagnetic resonance linewidth in NiO/Pt and NiO/Pd, Phys. Rev. B **101**, 060402(R) (2020).

[10] A. V. Kimel, B. A. Ivanov, R. V. Pisarev, P. A. Usachev, A. Kirilyuk, and T. Rasing, Inertia-driven spin switching in antiferromagnets, Nat. Phys. **5**, 727 (2009).

[11] S. Schlauderer, C. Lange, S. Baierl, T. Ebnet, C. P. Schmid, D. C. Valovcin, A. K. Zvezdin, A. V. Kimel, R. V. Mikhaylovskiy, and R. Huber, Temporal and spectral fingerprints of ultrafast all-coherent spin switching, Nature **569**, 383 (2019).

[12] H. J. Juretschke, Electromagnetic theory of dc effects in ferromagnetic resonance, J. Appl. Phys. **31**, 1401 (1960).

[13] W. G. Egan and H. J. Juretschke, Dc detection of ferromagnetic resonance in thin nickel films, J. Appl. Phys. **34**, 1477 (1963).

[14] N. Mecking, Y. S. Gui, and C. M. Hu, Microwave photovoltage and photoresistance effects in ferromagnetic microstrips, Phys. Rev. B **76**, 224430 (2007).

[15] H. Mizuno, T. Moriyama, M. Kawaguchi, M. Nagata, K. Tanaka, T. Koyama, D. Chiba, and T. Ono, Ferromagnetic resonance measurements in sub-nanometer Fe films, Appl. Phys. Express **8**, 073003 (2015).

[16] Luqiao Liu, Takahiro Moriyama, D. C. Ralph, and R. A. Buhrman, Spin-Torque Ferromagnetic Resonance Induced by the Spin Hall Effect, Phys. Rev. Lett. **106**, 036601 (2011).

[17] E. Saitoh, M. Ueda, and H. Miyajima, Conversion of spin current into charge current at room temperature: Inverse spin-Hall effect, Appl. Phys. Lett. **88**, 182509 (2006).

[18] H. Nakayama, K. Ando, K. Harii, T. Yoshino, R. Takahashi, Y. Kajiwara, K. Uchida, Y. Fujikawa, and E. Saitoh, Geometry dependence on inverse spin Hall effect induced by spin pumping in $Ni_{81}Fe_{19}$/Pt films, Phys. Rev. B **85**, 144408 (2012).

[19] J. Li, C. B. Wilson, R. Cheng, M. Lohmann, M. Kavand, W. Yuan, M. Aldosary, N. Agladze, P. Wei, M. S. Sherwin, and J. Shi, Spin current from sub-terahertz-generated antiferromagnetic magnons, Nature **578**, 70 (2020).

[20] P. Vaidya, S. A. Morley, J. van Tol, Y. Liu, R. Cheng, A. Brataas, D. Lederman, and E. del Barco, Subterahertz spin pumping from an insulating antiferromagnet, Science **368**, 160 (2020).

[21] T. Idehara and S. P. Sabchevski, Gyrotrons for high-power terahertz science and technology at FIR UF, J. Infrared, Millimeter, Terahertz Waves **38**, 62 (2017).

[22] A. Fisher, Y. Park, M. Lenz, A. Ody, R. Agustsson, T. Hodgetts, A. Murokh, and P. Musumeci, Single-pass high-efficiency terahertz free-electron laser, Nat. Photonics **16**, 441 (2022).

[23] C. D. Stanciu, A. v Kimel, F. Hansteen, A. Tsukamoto, A. Itoh, and A. Kirilyuk, Ultrafast spin dynamics across compensation points in ferrimagnetic GdFeCo: The role of angular momentum compensation, Phys. Rev. B **73**, 220402(R) (2006).

[24] C. Kim, S. Lee, H. G. Kim, J. H. Park, K. W. Moon, J. Y. Park, J. M. Yuk, K. J. Lee, B. G. Park, S. K. Kim, *et al.*, Distinct handedness of spin wave across the compensation temperatures of ferrimagnets, Nat. Mater. **19**, 980 (2020).

[25] K. J. Kim, S. K. Kim, Y. Hirata, S. H. Oh, T. Tono, D. H. Kim, T. Okuno, W. S. Ham, S. Kim, G. Go, *et al.*, Fast domain wall motion in the vicinity of the angular

momentum compensation temperature of ferrimagnets, Nat. Mater. **16**, 1187 (2017).

[26] L. Caretta, M. Mann, F. Büttner, K. Ueda, B. Pfau, C. M. Günther, P. Hessing, A. Churikova, C. Klose, M. Schneider, *et al.*, Fast current-driven domain walls and small skyrmions in a compensated ferrimagnet, Nat. Nanotechnol. **13**, 1154 (2018).

[27] Y. Hirata, D. H. Kim, S. K. Kim, D. K. Lee, S. H. Oh, D. Y. Kim, T. Nishimura, T. Okuno, Y. Futakawa, H. Yoshikawa, *et al.*, Vanishing skyrmion Hall effect at the angular momentum compensation temperature of a ferrimagnet, Nat. Nanotechnol. **14**, 232 (2019).

[28] K. Ueda, M. Mann, P. W. P. de Brouwer, D. Bono, and G. S. D. Beach, Temperature dependence of spin-orbit torques across the magnetic compensation point in a ferrimagnetic TbCo alloy film, Phys. Rev. B **96**, 064410 (2017).

[29] J. Sinova, S. O. Valenzuela, J. Wunderlich, C. H. Back, and T. Jungwirth, Spin Hall effects, Rev. Mod. Phys. **87**, 1213 (2015).

[30] A. Hoffmann, Spin Hall effects in metals, IEEE Trans. Magn. **49**, 5172 (2013).

[31] M. Harder, Z. X. Cao, Y. S. Gui, X. L. Fan, and C. M. Hu, Analysis of the line shape of electrically detected ferromagnetic resonance, Phys. Rev. B **84**, 054223 (2011).

[32] T. A. Ostler, R. F. L. Evans, R. W. Chantrell, U. Atxitia, O. Chubykalo-Fesenko, I. Radu, R. Abrudan, F. Radu, A. Tsukamoto, A. Itoh, *et al.*, Crystallographically amorphous ferrimagnetic alloys: Comparing a localized atomistic spin model with experiments, Phys. Rev. B **84**, 024407 (2011).

[33] B. I. Min and Y. R. Jang, The effect of the spin-orbit interaction on the electronic structure of magnetic materials, J. Phys.: Condens. Matter **3**, 5131 (1991).

[34] F. Schlickeiser, U. Atxitia, S. Wienholdt, D. Hinzke, O. Chubykalo-Fesenko, and U. Nowak, Temperature dependence of the frequencies and effective damping parameters of ferrimagnetic resonance, Phys. Rev. B **86**, 214416 (2012).

[35] G. P. Rodrigue, H. Meyer, and R. V. Jones, Resonance measurements in magnetic garnets, J. Appl. Phys. **31**, S376 (1960).

[36] S. K. Kim, K. Lee, and Y. Tserkovnyak, Self-focusing skyrmion racetracks in ferrimagnets, Phys. Rev. B **95**, 140404(R) (2017).

[37] S. Funada, Y. Shiota, M. Ishibashi, T. Moriyama, and T. Ono, Enhancement of spin wave group velocity in ferrimagnets with angular momentum compensation, Appl. Phys. Express **13**, 063003 (2020).

[38] S. K. Kim, Y. Tserkovnyak, and O. Tchernyshyov, Propulsion of a domain wall in an antiferromagnet by magnons, Phys. Rev. B **90**, 104406 (2014).

[39] See the Supplemental Material at http://link.aps.org/supplemental/10.1103/PhysRevApplied.19.L031003 for estimations of the magnetic susceptibility at f_L and f_R.

[40] A. G. Gurevich and G. A. Melkov, *Magnetization oscillations and waves* (CRC Press, Boca Raton, FL, USA, 1996).

[41] A. Kamra, R. E. Troncoso, W. Belzig, and A. Brataas, Gilbert damping phenomenology for two-sublattice magnets, Phys. Rev. B **98**, 184402 (2018).

[42] J. Seib and M. Fähnle, Calculation of the Gilbert damping matrix at low scattering rates in Gd, Phys. Rev. B **82**, 064401 (2010).

[43] T. G. A. Verhagen, H. N. Tinkey, H. C. Overweg, M. van Son, M. Huber, J. M. van Ruitenbeek, and J. Aarts, Temperature dependence of spin pumping and Gilbert damping in thin Co/Pt bilayers, J. Phys.: Condens. Matter **28**, 056004 (2016).

[44] N. H. Duc and D. Givord, Exchange interactions in amorphous Gd-Co alloys, J. Magn. Magn. Mater. **157**, 169 (1996).

[45] M. Huang, M. U. Hasan, K. Klyukin, D. Zhang, D. Lyu, P. Gargiani, M. Valvidares, S. Sheffels, A. Churikova, F. Büttner, *et al.*, Voltage control of ferrimagnetic order and voltage-assisted writing of ferrimagnetic spin textures, Nat. Nanotechnol. **16**, 981 (2021).